Assessment of the mean glandular dose using LiF:Mg,Ti, LiF:Mg,Cu,P, $Li_2B_4O_7$:Mn and $Li_2B_4O_7$:Cu TL detectors in mammography radiation fields

2016 Phys. Med. Biol. 61 6384

(http://iopscience.iop.org/0031-9155/61/17/6384)

IOP Publishing | Institute of Physics and Engineering in Medicine Physics in Medicine & Biology

Phys. Med. Biol. **61** (2016) 6384–6399 doi:10.1088/0031-9155/61/17/6384

Assessment of the mean glandular dose using LiF:Mg,Ti, LiF:Mg,Cu,P, $Li_2B_4O_7$:Mn and $Li_2B_4O_7$:Cu TL detectors in mammography radiation fields

M J Fartaria[1,2,7], C Reis[2,3], J Pereira[1,4], M F Pereira[1,4], J V Cardoso[1], L M Santos[1], C Oliveira[1,4], V Holovey[5], A Pascoal[2,6] and J G Alves[1,4]

[1] Instituto Superior Técnico (IST), Universidade de Lisboa (UL), Laboratório de Proteção e Segurança Radiológica (LPSR), Estrada Nacional 10 (ao km 139,7), 2986-066 Bobadela, Portugal
[2] Universidade Católica Portuguesa, Faculdade de Engenharia, Estrada Octávio Pato, 2635-631, Rio de Mouro, Portugal
[3] Escola Superior de Tecnologia da Saúde de Lisboa (ESTESL), Av. D. João II, Lote 4.69.01, 1990-096 Lisboa, Portugal
[4] Centro de Ciências e Tecnologias Nucleares (C2TN) do IST, UL, EN 10 (ao km 139,7), 2986-066 Bobadela, Portugal
[5] Institute of Electron Physics, Ukrainian Academy of Sciences, 21 Universitetska Str., 88017 Uzhgorod, Ukraine
[6] Department of Medical Engineering and Physics, King's College Hospital NHS Foundation Trust, London, UK

E-mail:mfartari@unil.ch

Received 18 December 2015, revised 12 April 2016
Accepted for publication 8 July 2016
Published 8 August 2016

Abstract

The aim of this paper is the characterization of four thermoluminescence detectors (TLD), namely, LiF:Mg,Ti, LiF:Mg,Cu,P, $Li_2B_4O_7$:Mn and $Li_2B_4O_7$:Cu for the measurement of the entrance surface air kerma (ESAK) and estimation of the mean glandular dose (MGD) in digital mammography examinations at hospitals and clinics. Low-energy x-ray beams in the typical energy ranges of mammography, produced with a tungsten target and additional 60 μm molybdenum filtration were implemented and characterized at the Laboratory of Metrology of Ionizing Radiation at Instituto Superior Técnico. These beams were used for the characterization of the TLDs in terms of sensitivity, linearity, reproducibility, energy dependence and fading

[7] Current address: Department of Radiology, Centre Hospitalier Universitaire Vaudois (CHUV) and University of Lausanne (UNIL), Lausanne, Switzerland.

at 40 °C. The energy dependence test was further extended using clinical beams produced by mammography units at hospitals and clinics. The method proposed by the International Atomic Energy Agency was used for the measurement of ESAK and assessment of MGD. The combined standard uncertainty for the measurement of ESAK (and MGD) was determined in accordance to the Guide to the expression of uncertainty in measurement. The x-ray beams generated in the 23–40 kV_p range presented HVL values from 0.36 to 0.46 mm Al. The beam produced at 28 kV_p (HVL 0.39 mm Al) was considered as reference. The radiation field defined a circle with 84 mm diameter with a maximum variation of the beam intensity of less than 1% at the top flat (plateau) within 4 cm of the central axis. The estimated total uncertainty for the measurement of air kerma was 0.42%. All the TL detectors tested showed good performance except the commercial $Li_2B_4O_7$:Mn (or TLD-800) which was excluded due to its poor sensitivity in our experimental set up. Both lithium fluorides showed better linearity and reproducibility as well as lower energy dependence and fading when compared to lithium borates. The stable behaviour of LiF:Mg,Ti and LiF:Mg,Cu,P detectors is reflected in the low combined standard uncertainty of ±5.6% and ±4.3% respectively (or ±5.1% and ±3.6% if fading is neglected). In general a total combined uncertainty lower than ±10% for the measurement of ESAK was obtained for the four TL materials studied.

Keywords: mammography, radiation quality, dosimetry, thermoluminescence, radiation dose assessment

1. Introduction

Mammography examination is the main method for the diagnostic of breast cancer and the main imaging modality internationally recommended for breast screening survey programs (Tung *et al* 2010, Camargo-Mendonza *et al* 2011, Sree *et al* 2011). The safe use of mammography requires a thorough quality assurance programme which addresses technical and clinical aspects and various guidance documents currently exist (IAEA 2011, Reis *et al* 2013). Mammography uses low energy x-ray beams to enhance the differential attenuation of breast tissues and breast lesions and to increase contrast (Bushberg *et al* 2002). In mammography the quantity of interest that relates to risk is the mean glandular dose (MGD). MGD is derived from the entrance surface air kerma (ESAK) modified by conversion factors (Dance *et al* 2000) that take into account the target and filter combination (T/F), the half-value layer (HVL) of the x-ray beam, as well as characteristics of the breast, namely compressed breast thickness and composition (proportion of glandular tissue).

The IEC 61267 standard (IEC 61267 2005) and IAEA Technical Report Series no. 457 (IAEA 2006) recommend the use of the RQR-M and RQA-M beam series as reference radiation beams for mammography produced with x-ray tubes with a molybdenum target and filter combination (or Mo/Mo). At the laboratory for metrology of ionizing radiation (LMRI) at Instituto Superior Técnico (IST) the x-ray tube available to produce low-energy x-ray beams operates with a tungsten target, a situation common to a large number of metrology laboratories. Taking into account this reality Kessler (2006) at the *Bureau International des Poids et Mesures* (BIPM) suggested an alternative method to produce reference beams

for mammography based on similar low-energy x-ray beams produced with a W target and additional 60 μm Mo filtration (or W/Mo). Moreover, the European Protocol on Dosimetry in Mammography (EUR 16263 1996) recommends that thermoluminescence (TL) detectors should be calibrated with a radiation beam quality (HVL) as close as possible to 0.4 mm Al and this was also considered.

Thermoluminescence dosimetry (TLD) is an interesting method for dosimetry in medical applications due to the small size of the detectors and their low effective atomic number (Z_{eff}) similar to that of soft biological tissues $Z_{eff} = 7.4$ (Horowitz 1984, McKeever 1985, Kron 1999, Zoetelief *et al* 2000, IAEA 2006). TL detectors of the lithium fluoride $Z_{eff} = 8.14$ and lithium borate $Z_{eff} = 7.4$ families were used for this study. Commercial samples of LiF:Mg,Ti, LiF:Mg,Cu,P and $Li_2B_4O_7$:Mn, commonly known as TLD-100, TLD-100H and TLD-800, respectively, as well as single crystals of $Li_2B_4O_7$:Mn and $Li_2B_4O_7$:Cu were used. In the selection of these materials factors like reliability of TLD-100, hypersensitivity of TLD-100H and potential low energy dependence of TLD-800 were taken into account (Horowitz 1984, McKeever *et al* 1995, Hsu *et al* 2008, Tung *et al* 2010).

In this paper the results obtained in the characterization of the radiation fields at LMRI and the characterization of lithium fluoride and borate TL dosemeters in terms of linearity, reproducibility, energy dependence in clinical fields and fading are presented. The methodology suggested by the IAEA (2006) was used for the measurement of ESAK and MGD and related uncertainty assessment.

2. Materials and methods

2.1. Characterization and dosimetry of the radiation beam

The low-energy x-ray tube available at LMRI is a Philips model MCN-165 type. The radiation beam was characterized in terms of field size (Oliveira *et al* 2015), homogeneity, HVL and dosimetry (Oliveira *et al* 2012) and the results were compared with requirements of standard protocols (ISO 4037-1 1996, IAEA 2006, Kessler 2006). A lead collimator with 18.2 mm diameter opening was designed, constructed and placed before the transmission ionization chamber (PTW model 7861) to monitor the beam and meet the dimensions defined in the calibration certificate of the parallel-plate ionization chamber. A cylindrical ionization chamber (PTW model 23331) was used to scan the measurement plane normal to the central axis of the radiation field, horizontally and vertically. Sets of high-purity Al filters (>99.9%, from Goodfellow, USA) were used to determine the HVL following the method described in the ISO 4037-1 standard (ICRU Report 10b 1964, ISO 4037-1 1996). A parallel-plane ionization chamber (PTW model 34068) calibrated at BIPM was used for the measurement of air kerma, taking into account pressure, temperature and humidity corrections for environmental reference conditions. The experimental setup used is presented in figure 1.

2.2. Characterization of TL detectors

Tissue equivalent TL detectors of the lithium fluoride and borate families were investigated for use in low-energy x-ray fields typical of mammography beams. All detectors followed an initialization procedure before being considered ready for use which consisted of three irradiation and readout cycles using a $^{90}Sr/^{90}Y$ irradiator (Vinten, UK). The detectors were readout in a Harshaw 4500 reader (Thermo Electron Corporation, Ohio, USA) following linear heating cycles with optimized time-temperature profile (TTP) parameters determined for each type (table 1).

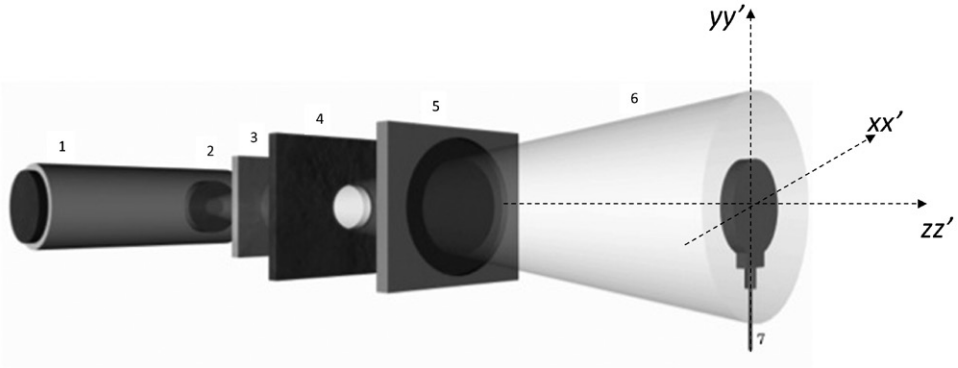

Figure 1. Experimental set-up: (1) x-ray tube; (2) side window; (3) additional filtration of 0.06 mm molybdenum; (4) lead collimator with a 18.2 mm aperture; (5) monitor ionization chamber; (6) x-ray beam cone; (7) plane-parallel ionization chamber placed at the measurement plane defined at a window to detector distance of 50 cm.

Table 1. Parameters for the readout and annealing cycle used for each detector studied.

Detector type:	LiF:Mg,Ti (TLD-100)	LiF:Mg,Cu,P (TLD-100H)	$Li_2B_4O_7$:Cu (sc)	$Li_2B_4O_7$:Mn (TLD-800, sc)
Reading cycle (TTP)				
Linear heating rate ($°C \cdot s^{-1}$)	5	5	8	8
Maximum temperature (°C)	300	255	300	300
Time at max. temperature (s)	6	10	3	3
Annealing cycle				
High temperature, time	400 °C, 60 min	240 °C, 10 min	300 °C, 15 min	300 °C, 15 min
Cooling rate	Natural	Natural	Natural	Natural
Low temperature, time	100 °C, 2 h	NA	NA	NA
Pre-readout temperature, time	100 °C, 10 min	130 °C, 10 min	100 °C, 5 min	100 °C, 5 min

NA—not applicable; sc—single crystal.

2.2.1. Readout and external annealing cycles and glow curve shapes. Standard annealing and readout cycles reported in the literature for each material were tested (Horowitz 1984, McKeever 1985, McKeever *et al* 1995). For each TL variety the parameters were selected with the aim to eliminate the low-temperature peaks with higher fading rates, produce a simplified glow curve composed of the main dosimetry peak(s) and smooth the glow curve analysis process. The need to reduce the re-use annealing time of a large quantity of detectors and simultaneously obtain an acceptable residual signal was also considered. In order to optimize the TL response and the quality of the glow curve for each material, the readout parameters (e.g. pre-heat temperature and time, heating rate, maximum readout temperature attained and time at maximum temperature) were studied.

2.2.2. Sample size. The commercial versions of LiF:Mg,Ti, LiF:Mg,Cu,P and $Li_2B_4O_7$:Mn, respectively known as TLD-100, TLD-100H and TLD-800 rods, with $6 \times 1 \times 1\,mm^3$ dimensions from Thermo Electronic Corporation (Ohio, USA) were used. Single crystal samples of

$Li_2B_4O_7$:Mn and $Li_2B_4O_7$:Cu with approximate dimensions of $5 \times 5 \times 1\,mm^3$ were also used, kindly provided by the Institute of Electron Physics of the Ukrainian Academy of Sciences (Uzhgorod, Ukraine). The number of dosemeters of each available material varied considerably. For the commercial detectors, three hundred TLD-100 were used and sixty for both TLD-100H and TLD-800. For the single crystals only seven samples of each type were available. The LiF materials will be considered as reference materials and deserved special attention.

2.2.3. Efficiency correction coefficients. Three annealing, irradiation and readout cycles specific to each detector type were performed. The final individual efficiency correction coefficient (ECC) was derived from the average of the three ecc obtained in each cycle.

2.2.4. Irradiations at LMRI. Except when otherwise stated all irradiations for the characterization studies were performed at LMRI using an x-ray beam produced with 28 kV_p tube voltage and W/Mo target and filter combination with 4 mGy in terms of air kerma free in air. Plastic sachets (0.13 mm thick) of $1 \times 3\,cm^2$ size were prepared containing samples of all TLD varieties, e.g. six rods of each type for TLD-100, TLD-100H and TLD-800 and one sample of each single crystal. The centre of the plastic sachet was positioned in the centre of the x-ray beam so that all detectors were simultaneously irradiated in order to produce results that are directly comparable.

2.2.5. Linearity. Irradiations were performed at 0.3, 0.5, 1.0, 2.0, 4.0, 8.0, 10.0, 12.0 and 15.0 mGy. This range was selected as it is representative of a range of ESAK values found in digital mammography examinations (Warren-Forward and Duggan 2004). The parameters of the linear fit were also used to determine the reader calibration factors (RCF) for each material. In the case of LiF materials, the irradiations were repeated at different periods to evaluate eventual sensitivity losses.

2.2.6. Reproducibility. For each TL material five readout, irradiations with 4 mGy and anneal cycles were performed.

2.2.7. Energy dependence at LMRI. In a second experiment the tube potential was set at 25, 28, 30, 35 and 40 kV_p and the dosemeters irradiated at 8 mGy.

2.2.8. Fading. Three sets of dosemeters were considered for each period of 4 and 8 d storage at 40 °C. The irradiation dose value was 4 mGy. The irradiation condition varied between all three sets: one was irradiated before the storage period, another one at the end of storage and the last one was not irradiated to control the background dose (Delgado *et al* 1992). Following the respective storage periods all three sets were readout at the same time. The storage temperature and periods were chosen in order to induce changes on full and empty traps, respectively, in irradiated and non-irradiated dosemeters (Alves *et al* 1999).

2.2.9. Energy dependence in clinical beams and cross calibration. Mammography sets used at clinical facilities produce x-ray beams with radiation qualities depending on the selected settings e.g. tube voltage, T/F combination and to a lesser extent on the equipment design. In all units the stability of the tube output was verified using a calibrated Unfors semiconductor dosemeter (formerly Unfors Instruments, presently Unfors RaySafe, Sweden). All possible variations in the response of the dosemeters for the different radiation qualities used at clinical facilities were taken into account. An energy dependence correction factor was established for each TL material and T/F combination based on the entrance surface air kerma measured with

the TL dosemeters and the Unfors reading. The results were normalized to the reference beam (28 kV_p and W/Mo).

2.2.10. Measurements at clinical facilities. Plastic sachets identical to the ones used for the irradiations at LMRI were prepared containing four rods of each type for TLD-100, TLD-100H and TLD-800 and one sample of each single crystal. The TL detectors were irradiated on the surface of a standard tissue-equivalent mammography phantom of semicircular PMMA slabs 45 mm thick, positioned at 4 cm from the chest wall detector edge and laterally centred (IAEA 2006). The ESAK is derived from the average of the measurements M (obtained from the dosemeter set ecc corrected and background subtracted), considering the specific RCF obtained for the W/Mo beam ($RCF_{W/Mo}$) modified by the k_Q, k_f and B factors that respectively represent the radiation quality, fading and backscatter factor, as shown in equation (1). k_Q is a factor that corrects for the difference in the response of the dosemeter calibrated at LMRI using the W/Mo beam and the quality Q delivered by the clinical beam produced by the mammography unit (IAEA 2006). According to the Dance method (Dance *et al* 2000), the MGD is obtained from the ESAK using two additional factors s and g, that respectively represent a spectral correction for the selected T/F combination and the correction for a breast 45 mm thick with 50% glandularity, as shown in equation (2).

$$\mathrm{ESAK} = \overline{M} \cdot \mathrm{RCF}_{\mathrm{W/Mo}} \cdot \frac{k_Q \cdot k_f}{B} \tag{1}$$

$$\mathrm{MGD} = \mathrm{ESAK} \cdot s \cdot g \tag{2}$$

3. Results and discussion

3.1. Characterization and dosimetry of the x-ray beams

An x-ray beam produced at 28 kV_p with W/Mo combination and 5 mA was used. The horizontal and vertical normalized air kerma profiles measured at 50 cm (tube window-to-detector distance) are presented in figure 2. The full width at half maximum defines a radiation field with 84 mm diameter. The maximum variation of the beam intensity measured at the plateau within 4 cm of the central axis of the beam is less than 1%. Variations of 1% and 3% were observed for the horizontal and for the vertical profiles, respectively, and the difference of 2% was due to the heel effect (Oliveira *et al* 2015).

The tube voltage selected varied from 23 to 50 kV_p. For each kV_p value the first HVL in terms of mm Al was determined and the results are shown in table 2. The average air kerma per monitor units and respective uncertainty as well as the effective energy derived from the HVL are also presented.

The HVL values obtained varied from 0.36 to 0.55 mm Al across the range of the tube voltages selected and the corresponding effective energies varied between 15.6 and 18.5 keV. It can be observed that for the range of tube voltages considered the HVL values are close to 0.4 mm Al, which is in agreement with the recommendations (EUR 16263 1996). The standard uncertainty for the measurement of air kerma listed in table 2 was estimated according to the Guide to the expression of uncertainty in measurement (BIPM 2009). All the factors with direct influence on the measurements were considered in the uncertainty assessment, classified into type A (statistical) and type B (other means of evaluation) categories, and are mentioned in table 3. For the type A uncertainties a normal probability distribution function (pdf) was considered whereas for the type B a rectangular pdf was taken into account. The estimated

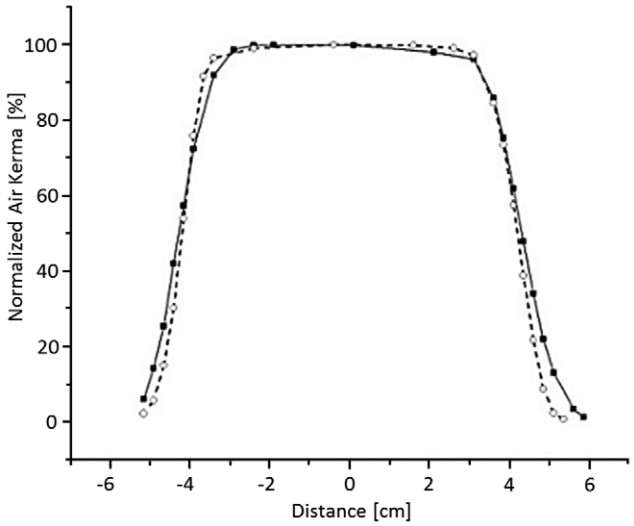

Figure 2. Radiation field size in terms of normalized air kerma at the measurement plane (window-to-detector distance of 50 cm): horizontal (open symbols and dashed line) and vertical (closed symbols and continuous line) profiles.

Table 2. Characterization and dosimetry of the x-ray beam produced with a W/Mo target and filter combination at different tube potentials: 1st HVL, air kerma per monitor units, respective uncertainty and effective energy.

Tube potential (kV_p)	Additional Mo filtration (mm)	1st HVL (mm Al)	Air kerma (mGy u.m.$^{-1}$)	Effective energy (keV)
23	0.06	0.359	8.012 ± 0.033	15.6
25	0.06	0.369	8.149 ± 0.034	15.8
28	0.06	0.387	8.182 ± 0.034	16.1
30	0.06	0.396	8.210 ± 0.034	16.2
35	0.06	0.427	8.252 ± 0.034	16.7
40	0.06	0.463	8.285 ± 0.034	17.3
50	0.06	0.549	8.416 ± 0.037	18.5

total uncertainty with a confidence level of 95% (or coverage factor, $k = 2$) was found to be 0.42%, well below the 3.2% maximum recommended value by the IAEA (2006).

3.2. Characterization of thermoluminescence detectors

3.2.1. Readout and external annealing cycles and glow curve shapes. The optimized readout, pre- and post-annealing cycle parameters listed in table 1 were always used for each TL detector. The glow curves obtained following irradiation to 4 mGy and readout with the respective TTP are shown in figure 3 for comparison: (a) LiF:Mg,Ti (TLD-100 rod), (b) LiF:Mg,Cu,P (TLD-100H rod), (c) $Li_2B_4O_7$:Mn (TLD-800 rod), (d) $Li_2B_4O_7$:Cu single crystal and (e) $Li_2B_4O_7$:Mn single crystal. For all materials studied it can be observed that the heating rates used (5 °C · s^{-1}and 8 °C · s^{-1}) produce full glow curves centred in the display, the main peak's maximum intensity is reached while the temperature is increasing and the main peak is fully emptied before the highest temperature in the TTP is attained. In the case of

Table 3. Uncertainty budget of air kerma true value at LMRI (all values in %).

Source of uncertainty	Type A (%)	pdf	Type B (%)	pdf
Parallel-plate ionization chamber:				
Measurement	0.006	Norm.	0.004	Rect.
Positioning			0.016	Rect.
Monitor chamber:				
Measurement	0.030	Norm.	0.008	Rect.
Temperature			0.010	Rect.
Air pressure			0.005	Rect.
Humidity			0.023	Rect.
Combined standard uncertainty for the experimental set up ($k = 2$)			0.09	
Combined standard uncertainty reported by the BIPM certificate ($k = 2$)			0.41	
Final combined standard uncertainty for irradiations at LMRI ($k = 2$)			0.42	

pdf—probability distribution function; Norm.—normal; Rect.—rectangular.

both LiF varieties, TLD-100H is nearly 10 times more sensitive than TLD-100. In the case of the borate single crystals with the same volume, $Li_2B_4O_7$:Cu seems to be nearly 5 times more sensitive than $Li_2B_4O_7$:Mn.

Comparing the similar shaped glow curves of both TL-800 rods and $Li_2B_4O_7$:Mn single crystal, the weak signal of the former was due to the different sensitive volume (rod to single crystal volume ratio of 6:25). The shift of the peak maximum towards higher temperatures observed in the single crystals was also ascribed to the larger sensitive volume in the single crystals and eventual higher thermal inertia. However, for the dose range used in our experiments (0.3–15 mGy) the TLD-800 rods showed an unstable and weak TL-signal when compared to the TLD-100 rods that was attributed to its emission wavelength in the range of 600 nm (McKeever 1985, McKeever *et al* 1995) away from the optimum sensitivity of the photomultiplier tube (PMT) in our reader[8] around 420 nm. This did not affect the readouts of the other detectors with approximate maximum emission wavelengths of 425 nm for LiF:Mg,Ti, 410 nm for LiF:Mg,Cu,P and 368 nm for $Li_2B_4O_7$:Cu (McKeever 1985), nor the single crystal $Li_2B_4O_7$:Mn with large sensitive volume. The same PMT was used throughout the experiments and its gain was kept constant. As the use of TLD-800 rods did not prove efficient it was abandoned. In the remaining the results presented and discussed will refer to TLD-100 rods, TLD-100H rods, $Li_2B_4O_7$:Cu and $Li_2B_4O_7$:Mn single crystals in this order.

3.2.2. ECC distribution. The distributions of the ecc for each batch of TLD-100 and TLD-100H detectors is presented in figure 4, varying between 0.80–1.25 and 0.80–1.40, respectively. Gaussian distribution curves were determined despite the reduced batch size of the TLD-100H material, providing variabilities of 8 and 10%, for TLD-100 and TLD-100H, respectively. The larger value observed for TLD-100H was due to the lower number of detectors in the batch, e.g. 60 dosemeters compared to 300 of the TLD-100 batch. Due to the small number of the borate single crystals available their distribution is not presented.

[8] Hamamatsu, 'Photronics tubes and related products catalogue', Hamamatsu, Japan (2010).

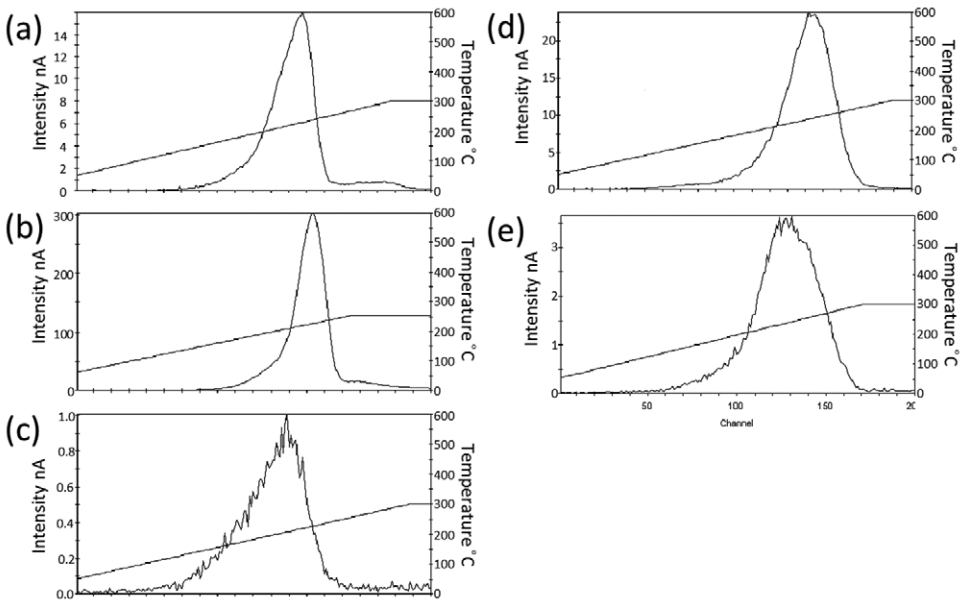

Figure 3. Time temperature profiles and glow curves of TL detectors irradiated in a x-ray beam with 28 kV_p and W/Mo combination to 4 mGy in terms of air kerma free in air, following the pre- and post-annealing cycles listed in table 1: (a) LiF:Mg,Ti (TLD-100 rods); (b) LiF:Mg,Cu,P (TLD-100H rods); (c) $Li_2B_4O_7$:Mn (TLD-800 rods); (d) $Li_2B_4O_7$:Cu single crystal and (e) $Li_2B_4O_7$:Mn single crystal.

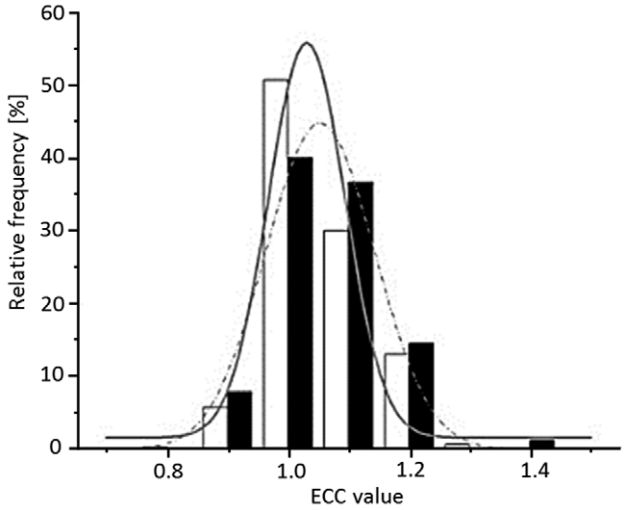

Figure 4. Distribution of the individual efficiency correction coefficients (ECC) for each batch: TLD-100 (white bars and continuous curve) and TLD-100H (dark bars and dashed curve).

3.2.3. Linearity. The results obtained in the range 0.3–15 mGy are presented in table 4. The fits are described by the slope, intercept and square of the correlation coefficient (R^2) obtained from linear regression analysis using the least square method. All materials showed a linear

Table 4. Linear regression parameters for each TL detector in the range 0.3–15 mGy.

TL material	Slope (mGy · nC^{-1})	Intercept (mGy)	R^2
TLD-100	0.037	1.3×10^{-4}	0.9993
TLD-100H	0.003	3.7×10^{-3}	0.9989
$Li_2B_4O_7$:Cu	0.032	–0.165	0.9967
$Li_2B_4O_7$:Mn	0.163	–0.400	0.9975

behaviour with good correlation as indicated by the R^2. For both LiF varieties the linearity measurements were repeated three times, at different stages, providing slopes (or RCF) that varied less than 3%.

As previously observed in the analysis of the glow curves, the RCF values obtained for each material indicate that TLD-100H is 10 times more sensitive than TLD-100 and in the case of the borate single crystals $Li_2B_4O_7$:Cu is 5 times more sensitive than $Li_2B_4O_7$:Mn. A simple comparison between fluorides and borates suggests that for the experimental setup used, $Li_2B_4O_7$:Mn is nearly 20 times less sensitive than TLD-100, while $Li_2B_4O_7$:Cu is as sensitive as TLD-100. However the volume of the single crystals is nearly 4 fold that of rods, that is, in our setup, $Li_2B_4O_7$:Cu is 4 times less sensitive than TLD-100. For the borates the linear regression does not intercept the origin and this was attributed to the reduced sample size, that is, while for fluorides the irradiated set consisted of six detectors, for the borates only one detector.

3.2.4. Reproducibility. The reproducibility of each TL type was measured for the reference beam (28 kV_p W/Mo, 4 mGy) and repeated 5 times. The results normalized to the average are shown in figure 5. All materials present a reproducible behaviour with variations within the intervals ±0.8, ±1.4, ±2.7 and ±3.4 of the mean respectively for TLD-100, TLD-100H, $Li_2B_4O_7$:Cu and $Li_2B_4O_7$:Mn. The reproducibility experiment as described herein was periodically checked and following 10 cycles a sensitivity decrease of around 2% and 4% was observed, respectively for TLD-100 and TLD-100H. These values were considered as inputs for the stability of the RCF in the uncertainty assessment.

3.2.5. Energy dependence at LMRI. In figure 6 the tube potential varied from 25 to 40 kV_p corresponding to a HVL between 0.37 and 0.47 mm Al, and in turn, to an effective energy between 15.8 and 17.3 keV. The dosemeters were irradiated with 8 mGy. The readings obtained were normalized to the average. In general, there is a higher variation on the results as compared to figure 5. There seems to be a tendency for an increase with the effective energy of the beam, particularly for the single crystal $Li_2B_4O_7$:Cu. Similar observations were indicated by Hsu *et al* (2008) and Tung *et al* (2010). Maximum variations observed were contained within the intervals ±2.3, ±1.8, ±6.3 and ±5.5%, respectively for TLD-100, TLD-100H, $Li_2B_4O_7$:Cu and $Li_2B_4O_7$:Mn. The signal to noise ratio measured following irradiations at 8 mGy represented 0.4%, 0.05%, 0.9% and 3.4% of the main signal for TLD-100, TLD-100H, $Li_2B_4O_7$:Cu $Li_2B_4O_7$:Mn, respectively.

3.2.6. Fading. The results obtained following storage at 40 °C are presented in figure 7. Closed symbols represent the dosemeter sets that were stored at 40 °C for 4 and 8 d after irradiation. The open symbols represent the other two sets stored at 40 °C for the same periods and irradiated prior to readout. The other sets were not irradiated and used to control background. All were readout at the same time and the results were normalized to prompt measurements.

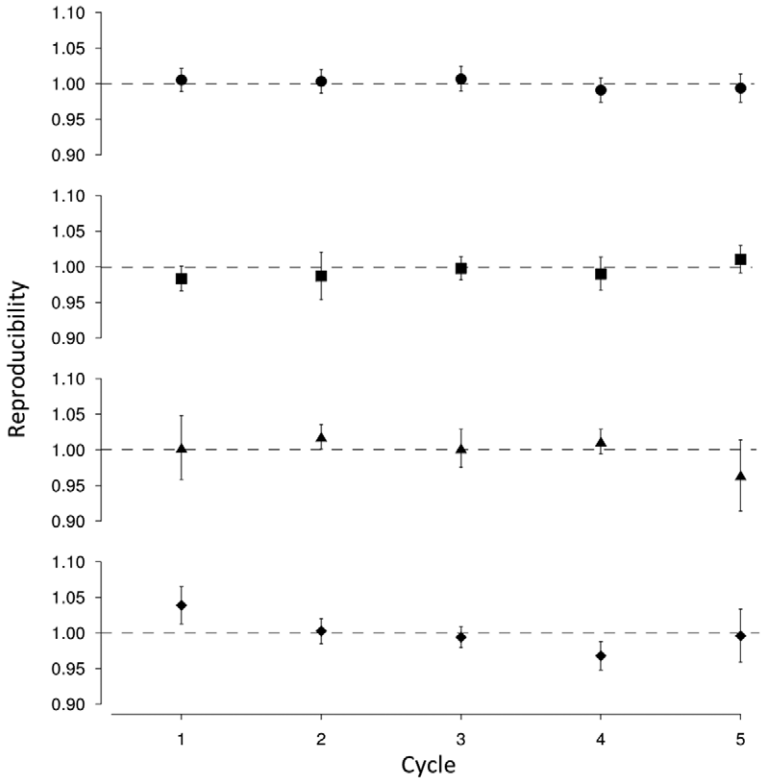

Figure 5. Reproducibility of TL detectors following 5 cycles (28 kV_p, W/Mo, 4 mGy). From top to bottom: TLD-100 (circle), TLD-100H (square), $Li_2B_4O_7$:Cu (triangle) and $Li_2B_4O_7$:Mn (rhombus).

Both lithium fluoride materials show small variations with storage at this temperature even for the longest storage period. The average variation observed was $\pm 2\%$ for 4 d storage and less than 4% for 8 d at 40 °C for TLD-100. These findings are supported by previous studies (Alves *et al* 1999, Pereira *et al* 2015). For the borate single crystals the average variation is higher, approximately -12% and -8% for $Li_2B_4O_7$:Cu for 4 and 8 d storage respectively, whilst the corresponding values for $Li_2B_4O_7$:Mn are -5% and -6%. $Li_2B_4O_7$:Mn appears more stable than $Li_2B_4O_7$:Cu, as suggested by other authors (McKeever 1985, McKeever *et al* 1995). Further work to investigate the effect of other storage temperatures and periods is being considered.

The workplace environment at our laboratory and at clinical facilities where the measurements were performed is temperature controlled around 22 °C. The dosemeters irradiated at the clinics were always readout on the day following the irradiations. The TTP and the re-use cycles were designed in order to avoid the influence of the low-temperature and high-fading rate peaks. On the other hand, the experiments were performed with storage periods at 40 °C and storage periods as long as 8 d suggestive of worst case scenarios. However such high temperatures were never attained during the field work for dose assessments. Taking these factors into consideration, this experiment allowed the characterization of the fading and sensitivity changes experienced by the TL materials. However it does not reflect a real situation endured by the detectors. Although the fading correction factor k_f was estimated and considered in the assessment of the total uncertainty budget, it was considered unnecessary for routine work.

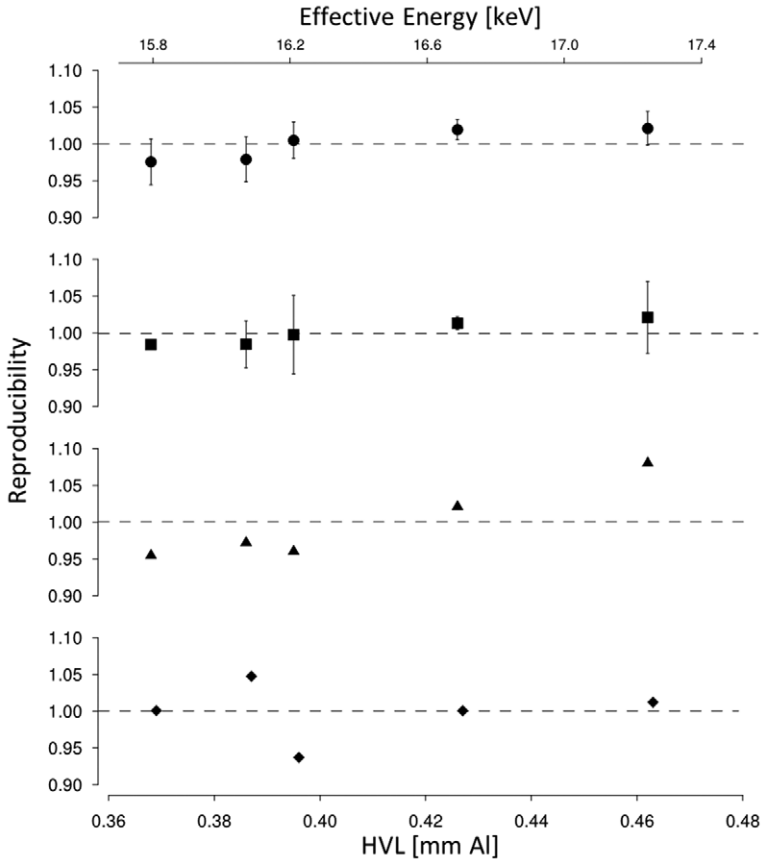

Figure 6. Energy dependence at LMRI (25–40 kV_p and W/Mo beam). From top to bottom: TLD-100 (circle), TLD-100H (square), $Li_2B_4O_7$:Cu (triangle) and $Li_2B_4O_7$:Mn (rhombus).

3.2.7. Energy dependence in clinical beams (cross calibration). The radiation qualities produced by dedicated mammography units differ from the reference beam used at LMRI mainly due to the different tube voltages and T/F combinations and, to a lesser extent, to variations in the design of the x-ray source. In order to take these aspects into account equation (1) considers k_Q a quality correction factor (cross calibration) (IAEA 2006). The k_Q factor was experimentally determined for each TL material using all the measurements performed at clinical facilities, for each T/F combination. In this way all possible variations due to the differences in tube voltages and equipment design were taken into account. At each clinical facility the stability of the tube output was verified with the Unfors dosemeter. All devices showed a stable behaviour with maximum variations lower than 1.4%. The TL materials were irradiated in automatic exposure control (AEC) mode and their reading in terms of ESAK compared to the Unfors dosemeter (cross calibration). The average k_Q obtained for each T/F combination and each TL material are presented in table 5 as well as the number of irradiations performed.

The uncertainty of the k_Q factor takes into account the different tube voltages and equipment design. All the beams were investigated with samples of fluorides and not so much with borates (due to the reduced sample size) and the k_Q factors obtained for TLD-100 and TLD-100H seem to be closer to unity. That for $Li_2B_4O_7$:Mn is farthest from unity while $Li_2B_4O_7$:Cu

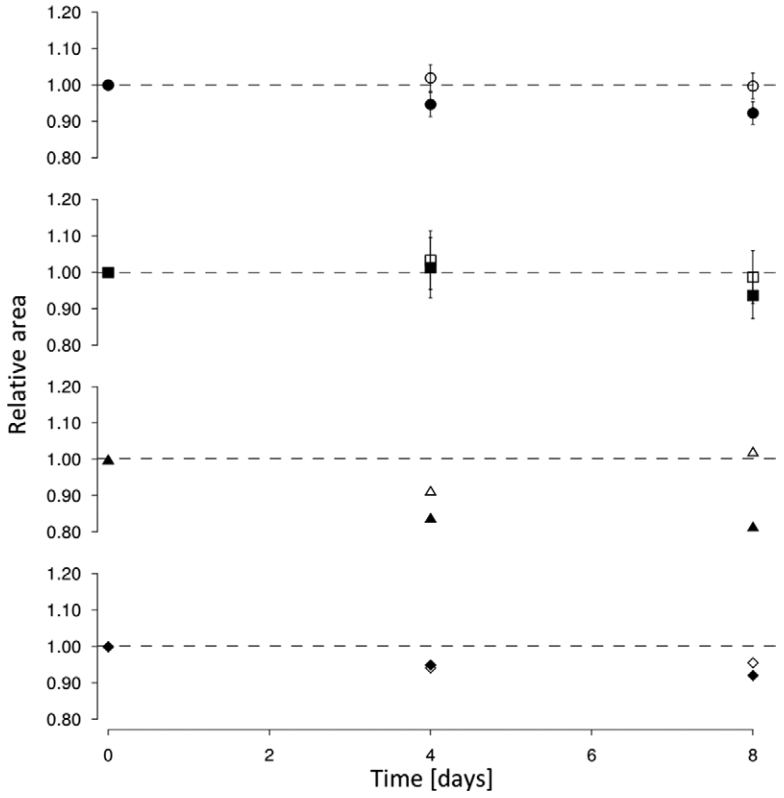

Figure 7. Fading and sensitivity changes following storage at 40 °C during 4 and 8 d. From top to bottom: TLD-100 (circle), TLD-100H (square), $Li_2B_4O_7$:Cu (triangle) and $Li_2B_4O_7$:Mn (rhombus). Closed and open symbols respectively represent storage after and before irradiation.

presents an intermediate behaviour. The largest uncertainty was observed for Rh/Rh quality which in our sample study was the less frequently used T/F combination.

3.2.8. Uncertainty of the measurement of ESAK. The expression for the measurement of ESAK is given by equation (1) and in the assessment of the combined standard uncertainty listed in table 6 the Guide (BIPM 2009) and the assumptions described below were considered.

The contribution to the uncertainty due to the measurements of the TL readout is in the 4th decimal digit generally of the order of 10^{-3}% and was neglected when compared to the other components. The TL readout is then corrected by the respective ecc and background subtracted to obtain the average $\overline{M}$. The TL sets were all composed at random so it is considered that the contributions to the uncertainty due to the dispersion of the TL sets are included in the RCF. The component to the uncertainty due to the $RCF_{W/Mo}$ was derived from the linearity measurements, the reproducibility results obtained in figure 5, as well as its decrease with time, squared and summed. For this component a normal pdf was assumed. The k_Q component to the uncertainty is given for each material by the relative standard deviations derived from table 5. For the case of TLD-100 varied between ±1.0% and ±4.4%; for the TLD-100H material between ±1.4% and ±3.0%; for the $Li_2B_4O_7$:Cu single crystal between ±3.2% and ±7.9%; and for the $Li_2B_4O_7$:Mn material between ±2.2% and ±8.7%. The highest value was considered and rectangular probability distribution functions were assumed. The

Table 5. k_Q correction factors obtained for each type of TL material in clinical beams normalized to the reference beam (W/Mo) at LMRI (cross calibration) (IAEA 2006, Kessler 2006).

Target and filter combination	Number of cases $LiF–Li_2B_4O_7$	TLD-100	TLD-100H	$Li_2B_4O_7$:Cu	$Li_2B_4O_7$:Mn
Mo/Mo	14–9	1.03 ± 0.09	1.05 ± 0.03	1.11 ± 0.07	1.13 ± 0.06
Mo/Rh	6–4	1.05 ± 0.02	1.01 ± 0.04	1.06 ± 0.14	1.17 ± 0.04
Rh/Rh	3–3	1.03 ± 0.07	0.99 ± 0.06	1.01 ± 0.16	1.15 ± 0.20
W/Rh	8–4	1.01 ± 0.06	0.92 ± 0.03	1.07 ± 0.11	1.15 ± 0.09

Table 6. Uncertainty budget for the estimate of ESAK.

Source of uncertainty	pdf	TLD-100	TLD-100H	$Li_2B_4O_7$:Cu	$Li_2B_4O_7$:Mn
Reproducibility	Normal	0.3	0.5	0.9	1.1
Linearity and stability, $RCF_{W/Mo}$	Normal	1.2	1.7	ND	ND
Energy dependence, k_Q (worst case)	Rectangular	2.5	1.7	4.6	5.0
Fading correction, k_f	Rectangular	1.2	1.2	6.9	2.9
Backscatter factor, B	Rectangular	0.2	0.2	0.2	0.2
Combined uncertainty, ($k = 2$)		5.6	4.3	16.7	11.8
Combined uncertainty, excl fading ($k = 2$)		5.1	3.6	9.3	10.3

pdf—probability distribution function; ND—not determined.

contribution to the uncertainty due to the backscatter factor B was determined taking into account its dependence on the HVL of the mammography beams that varied between 0.313 and 0.575 mm Al. In this range the corresponding tabulated B factors (IAEA 2006) showed a linear behaviour varying from 1.08 to 1.12. According to the calibration certificate of the Unfors dosemeter an uncertainty of 5% is expected which corresponds to an uncertainty in the determination of the B factor of $\pm 0.3\%$. For this deviation a rectangular probability distribution function was assumed. The k_f component to the uncertainty was derived from the results in figure 7. However, taking into account that dosemeters were always irradiated and read the following day, the contribution to fading can be neglected.

As explained throughout this paper there is more information for the fluorides than for the borates. The total combined uncertainty with a confidence interval of 95% is then 5.1% and 3.6%, respectively for TLD-100 and TLD-100H. These values are well below $\pm 10\%$ recommended by the IAEA (2006) and the European Commission (EUR 16263 1996) for the measurement of ESAK. For the single crystals it is somehow higher, around 9.3% and 10.3%, respectively for $Li_2B_4O_7$:Cu and $Li_2B_4O_7$:Mn but still acceptable and in accordance to the guidance documents.

3.2.9. Assessment of MGD. In figure 8 four estimates of MGD obtained as described herein are presented, each obtained in different mammography units and irradiated with different radiation qualities or T/F combinations.

For the uncertainty in the measurement of the MGD the values mentioned in table 6 were considered combined with the uncertainty in the g factor of $\pm 2.6\%$ assuming a rectangular pdf, yielding a combined standard uncertainty of 7.3%, 6.4%, 10.7% and 11.5%, respectively

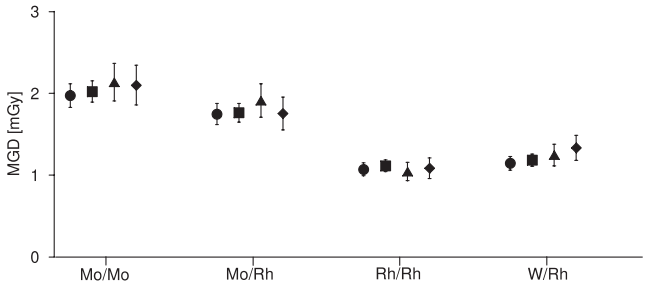

Figure 8. Four mean glandular dose measurements obtained with TL detectors in mammography units operated in AEC mode. The uncertainty bars were obtained as described in the text. From left to right: Mo/Mo, Mo/Rh, Rh/Rh and W/Rh combinations. TLD-100 (circle), TLD-100H (square), $Li_2B_4O_7$:Cu (triangle) and $Li_2B_4O_7$:Mn (rhombus).

for TLD-100, TLD-100H, $Li_2B_4O_7$:Cu and $Li_2B_4O_7$:Mn. For each radiation quality it can be observed that the MGD values obtained with each TL variety are close and all within the measurement uncertainties. As expected, the larger uncertainty values correspond to the borates.

4. Conclusion

At LMRI a reference x-ray beam produced with a W target, additional Mo filtration and operated in the low energy range typical of mammography was implemented using the method suggested by BIPM (Kessler 2006). The combined uncertainty for the measurement of air kerma free in air was 0.42%. The beams produced at LMRI were used for the characterization of four tissue equivalent TL detectors of LiF:Mg,Ti (TLD-100), LiF:Mg,Cu,P (TLD-100H), $Li_2B_4O_7$:Cu and $Li_2B_4O_7$:Mn for use in mammography radiation fields. The dosemeters were characterized in terms of linearity, reproducibility, energy dependence at LMRI, fading and energy dependence in clinical beams used for cross calibration, using TLD-100 and TLD-100H as reference materials. All parameters determined in the characterization process were taken into account and used in the assessment of the combined standard uncertainty for the measurement of ESAK (and MGD) according to the Guide to the expression of uncertainty in measurement. The method for the assessment of ESAK and further MGD in dedicated mammography units at hospitals and private clinics was tested and examples are provided.

All dosemeter materials tested are adequate to the measurement of ESAK and estimate of MGD. Taking into consideration a total combined uncertainty lower than $\pm 10\%$ for ESAK the best results were obtained with LiF:Mg,Cu,P (TLD-100H) followed by LiF:Mg,Ti (TLD-100), although both single crystals provided also reasonable results. On the one hand a more thorough study was performed with both fluoride materials than with the borate single crystals, however the sample size of the latter conditioned the uncertainty assessment. Despite this fact, the four materials seem adequate for use in mammography dose assessment.

Acknowledgment

This work was partly funded by Fundação para a Ciência e a Tecnologia (FCT, Portugal) with a research grant under the framework of project ref. PTDC/SAU-BEB/100745/2008 awarded to MJ Fartaria.

References

Alves J G, Muñiz J L, Gómez-Rós J M and Delgado A 1999 A comparative study on the thermal stability of LiF:Mg,Ti and LiF:Mg,Cu,P detectors for environmental monitoring *Radiat. Prot. Dosim.* **85** 235–57

BIPM 2009 *Evaluation of Measurement Data—an Introduction to the Guide to the Expression of Uncertainty in Measurement and Related Documents* (Sèvres: Joint Committee for Guides in Metrology)

Bushberg J T, Seibert J A, Leidholdt E M and Boone J M 2002 Mammography *The Essential Physics of Medical Physics of Medical Imaging* (Philadelphia, PA: Lippincott Williams & Wilkins) pp 191–229

Camargo-Mendoza R E, Poletti M E, Costa A M and Caldas L V E 2011 Measurement of some dosimetric parameters for two mammography systems using thermoluminescent dosimetry *Radiat. Meas.* **46** 2086–9

Dance D R, Skinner C L, Young K C, Becket J R and Kotre C J 2000 Additional factors for the estimation of mean glandular breast dose using the UK mammography dosimetry protocol *Phys. Med. Biol.* **45** 3225–40

Delgado A, Gómez Ros J M and Muñiz J L 1992 Temperature effects in LiF TLD-100 based environmental dosimetry *Radiat. Prot. Dosim.* **45** 101–5

EUR 16263 1996 *European Protocol for Dosimetry in Mammography* (Luxembourg: Office for Publications of the European Communities)

Horowitz Y 1984 *Thermoluminescence and Thermoluminescent Dosimetry* vol I and II (Boca Raton, FL: CRC)

Hsu G C, Tsai H Y, Chu C H and Yiou S M 2008 Energy responses and visibility for thin film-thermoluminescent dosimeters in mammography *Radiat. Meas.* **43** 964–7

IAEA 2006 Dosimetry in diagnostic radiology: an international code of practice *IAEA Technical Reports Series* No. 457 International Atomic Energy Agency, Vienna

IAEA 2011 Quality assurance programme for digital mammography *IAEA Human Health Series* No 17 International Atomic Energy Agency, Vienna

ICRU Report 10b 1964 Physical aspects of irradiation *National Bureau of Standards Handbook 85* (Bethesda, MD: International Commission of Radiation Units and Measurements)

IEC 61267 2005 *Medical Diagnostic X-ray Equipment—Radiation Conditions for Use in the Determination of Characteristics* (Geneva: International Electrotechnical Commission)

ISO 4037-1 1996 *X and Gamma Reference Radiation for Calibrating Dosemeters and Dose Rate Meters and for Determining their Response as a Function of Photon Energy—Part 1* (Geneva: International Organization for Standardization)

Kessler C 2006 Establishment of simulated mammography radiation qualities at the BIPM *Report* BIPM-06/08 Bureau International des Poids et Mesures, Sèvres

Kron T 1999 Applications of thermoluminescence dosimetry in medicine *Radiat. Prot. Dosim.* **85** 333–40

McKeever S W S 1985 *Thermoluminescence of Solids* (Cambridge: Cambridge University Press)

McKeever S W S, Moscovitch M and Townsend P D 1995 *Thermoluminescence Dosimetry Materials—Properties and Uses* (Kent: Nuclear Technology Publishing)

Oliveira A D, Fartaria M J, Cardoso J V, Santos L M, Oliveira C, Pereira M F and Alves J G 2015 The determination of the focal spot size of an x-ray tube from the radiation beam profile *Radiat. Meas.* **82** 138–45

Oliveira C, Cardoso J, Santos L, Limede P, Góis D and Oliveira M 2012 A dosimetria em radiodiagnóstico *Rev. Medições e Ensaios* **1** 29–42

Pereira J, Pereira M F, Rangel S, Saraiva M, Santos L M, Cardoso J V and Alves J G 2015 Fading effect of LiF:Mg,Ti and LiF:Mg,Cu,P ext-rad and whole-body detectors *Radiat. Prot. Dosim.* (doi: 10.1093/rpd/ncv445)

Reis C, Pascoal A, Sakellaris T and Koutalonis M 2013 Quality assurance and quality control in mammography: a review of available guidance worldwide *Insights Imaging* **4** 539–53

Sree S V, Ng E Y, Acharya R and Faust O 2011 Breast imaging: a survey *World J. Clin. Oncol.* **2** 171–8

Tung C J, Lin M T, Hsu F Y, Lee J H, Chu C H and Tsai H Y 2010 Half-value layer determination using thermoluminescent dosimeters for digital mammography *Radiat. Meas.* **45** 729–32

Warren-Forward H M and Duggan L 2004 Towards *in vivo* TLD dosimetry in mammography *Br. J. Radiol.* **77** 426–32

Zoetelief J, Julius H and Christensen P 2000 *Recommendations for Patient Dosimetry in Diagnostic Radiology Using TLD* (Luxembourg: Directorate-General for Research, European Comission)